Coordinated Voltage Control Scheme for VSC-HVDC Connected Wind Power Plants

Guo, Yifei; Gao, Houlei; Wu, Qiuwei; Zhao, Haoran; Østergaard, Jacob

Published in:
I E T Renewable Power Generation

Link to article, DOI:
10.1049/iet-rpg.2017.0344

Publication date:
2017

Document Version
Peer reviewed version

Coordinated Voltage Control Scheme for VSC-HVDC Connected Wind Power Plants

Yifei Guo [1], Houlei Gao [1*], Qiuwei Wu[1,2], Haoran Zhao[1], Jacob Østergaard [2]

[1] School of Electrical Engineering, Shandong University, Jinan 250061, People's Republic of China
[2] Department of Electrical Engineering, Technical University of Denmark, Lyngby, Denmark
[*] houleig@sdu.edu.cn

Abstract: This paper proposes a coordinated voltage control scheme based on model predictive control (MPC) for voltage source converter-based high voltage direct current (VSC-HVDC) connected wind power plants (WPPs). In the proposed scheme, voltage regulation capabilities of VSC and WTGs are fully utilized and optimally coordinated. Two control modes, namely operation optimization mode and corrective mode, are designed to coordinate voltage control and economic operation of the system. In the first mode, the control objective includes the bus voltages, power losses and dynamic Var reserves of wind turbine generators (WTGs). Only the terminal voltages of WTGs are taken into account in the second mode. The predictive model of the system including VSC and WTGs is developed firstly. The calculation of sensitivity coefficients is done by an analytical method to improve the computational efficiency. Simulation results are presented to demonstrate the effectiveness of the proposed controller and the control performance is compared with conventional optimal control and loss minimization control. Besides, the robustness of the proposed controller to communication time delay and measurement errors is investigated in the last.

1. Introduction

Wind power has become a major source of renewable energy. The European Wind Energy Association (EWEA) estimates that the installed capacity of wind power could expand to 320 GW by 2030 [1]. There seems to be a law of scale, which directs development to ever larger turbines located at greater distances to shore, at greater water depths and in larger parks. Due to the reactive charging currents and compensation need, conventional high voltage alternative current (HVAC) transmission through submarine cables becomes uneconomical as the distance from the shore increases. Hence, voltage source converter-based high voltage direct current (VSC-HVDC) is a more suitable solution for distant offshore wind power plants (WPPs) due to its flexible active and reactive power control, feasibility of multi-terminal dc or meshed grids and inherent black start capability [2-3].

The increasing penetration of wind power has created a great number of technical and economic challenges for the developers and operators due to variability and uncertainty of wind power [4]-[6]. In order to meet these challenges, grid code requirements have been specified for wind power integration, including voltage regulation and Var capabilities of WPPs [7].

For conventional AC connected WPPs, the transmission system operators (TSOs) have elaborated specific technical requirements for connecting the large WPPs, including reactive power, power factor and voltage control [8]. The voltage control mode often shows superior performance. A number of voltage control strategies have been proposed for WPPs [9]-[13]. In [9], the total required reactive power of a WPP was determined by the voltage of the point of connection (POC), and then dispatched to each wind turbine generator (WTG) based on a proportional allocation method according to the available reactive power of WTGs. Distributing the reactive power in a proportional way could be helpful to ensure a correct dynamic performance of the WTGs and a sufficient security level from their maintenance point of view. An optimal automatic voltage control strategy was designed and implemented in [10], which includes three different control modes considering all the terminal voltages of WTGs and dynamic Var reserves. In [11], an autonomous voltage control controller was designed for AC connected WPPs. The control strategy considers coordination of fast and slow Var devices as well as the on-load tap changer (OLTC) of transformers. The impacts of SVC/STATCOM on wind farm voltage regulation were investigated in [12]. The dynamic bifurcations induced by the limits of a wind farm voltage supervisory control was investigated in [13]. In general, most of the studies focused on the voltage at POC which is required by the system operators.

For HVDC connected offshore WPPs, the offshore WPPs are decoupled from the onshore AC grid. A considerable number of studies have been done for the fault ride through (FRT)/ low voltage ride through (LVRT) capability of offshore WPPs [14]-[16]. In [14], a novel configuration and transient management control strategy for VSC-HVDC system was proposed to provide smooth power transferring during fault condition. It can significantly improve the reliability of system during severe faults. In [15], a nine switch converter based configuration and control strategy for the VSC-HVDC connected offshore WPPs was proposed to enhance the FRT operation of the system. The effect of FRT behavior of VSC-HVDC connected offshore WPPs on AC/DC system dynamics was analyzed in [16].

Compared with the considerable number of studies for AC connected WPPs such as [9]-[13], few studies focused on the voltage regulation problem of HVDC connected WPPs. However, with the development of large-scale offshore wind projects, the Var/Voltage regulation problem inside offshore WPPs should be addressed. Generally, the WPP side VSC (WPPVSC) is required to operate as a voltage source with constant AC frequency and phase angle for the offshore AC grid. Most of the time, the voltage

reference of the VSC-controlled AC bus keeps constant at the nominal value [17], which does not take full advantage of the fast voltage regulation capability of VSC. Besides, the economical operation of offshore AC grid is not considered.

The main contribution of this paper is an attempt to take full use of the voltage regulation capability of the VSC and WTGs. A coordinated voltage control scheme based on model predictive control (MPC-CVCS) for VSC-HVDC connected offshore WPPs is proposed, which aims to maintain all bus voltages within the feasible range and simultaneously optimize the system operation under different wind conditions. The control of VSC and WTGs is optimally coordinated using the MPC method. An analytical sensitivity coefficient calculation method is used to improve the computation efficiency. Two different control modes are designed for different operation conditions to coordinate the voltage regulation and economical operation.

The rest of the paper is organized as follows. Section 2 briefly introduces the proposed coordinated voltage control method. In Section 3, the predictive model of the system including VSC and WTGs are presented. The analytical sensitivity coefficient calculation is described in Section 4. Section 5 presents the mathematical models of the MPC-CVCS. Simulation results along with discussions are presented in Section 6, followed by conclusions.

2. MPC based coordinated voltage control for VSC-HVDC connected WPPs

Fig. 1 shows the structure of the coordinated voltage control scheme. WTGs and VSC are optimally coordinated in the proposed voltage control scheme.

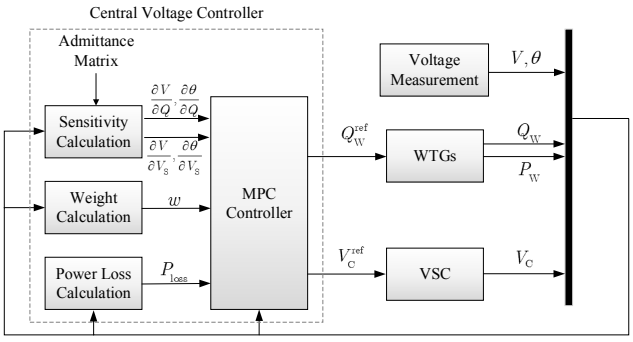

Fig. 1. *Structure of the MPC-CVCS.*

VSC has fast voltage regulation capability, which has been utilized for fast active power reduction during the FRT control. In the proposed voltage control scheme, the voltage reference of the VSC-controlled bus $V_{\mathrm{C}}^{\mathrm{ref}}$ is determined by the MPC controller.

Due to the considerable number of WTGs, the voltage regulation capability of WTGs should be also taken into account. The modern WTGs can be considered as good Var source in WPPs. They can track the Var reference $Q_{\mathrm{W}}^{\mathrm{ref}}$ given by the MPC controller. And the WTGs can effectively regulate all the bus voltages within the offshore AC grid.

In order to coordinate voltage control and economical operation, the voltage controller has two control modes: 1) optimization operation mode, and 2) corrective mode. In the first mode, all bus voltages are within the feasible range. The control objective is to minimize voltage deviations of the key buses, reduce active power losses and maximize the Var reserves of WTGs. In the corrective mode, the control objective is to correct the bus voltage which violates the limits. An adaptive weighting coefficient allocation method is used in this paper to regulate the voltage more effectively. The details are presented in Section 5.

3. Predictive model of WTGs and VSC

MPC is an optimization control method widely used in many industrial applications. It uses the receding horizon principle so that a finite-horizon optimal control problem is solved over a fixed interval of time. It is suitable for coordinating VSC and WTGs in voltage control. In this section, the discrete state-space models of VSC and WTGs are presented.

3.1. Predictive Model of WTGs

As mentioned above, the control commands sent by the MPC controller to WTGs are the reactive power references. Suppose the current reactive power measurement is Q_{W}^{0}, $\Delta Q_{\mathrm{W}}^{\mathrm{ref}} = Q_{\mathrm{W}}^{\mathrm{ref}} - Q_{\mathrm{W}}^{0}$ and $\Delta Q_{\mathrm{W}} = Q_{\mathrm{W}} - Q_{\mathrm{W}}^{0}$. If all the WTGs are controlled with reactive power control mode, the following turbine transfer function is obtained, which is considering a perfect control decoupling between the d-q axes [18],

$$\Delta Q_{\mathrm{W}} = \frac{1}{1+T_{\mathrm{W}}s}\Delta Q_{\mathrm{W}}^{\mathrm{ref}} \tag{1}$$

where T_{W} is the time constant, which is in the range of 1~10s [11]. The corresponding continuous-time predictive model of reactive power output for N_{W} WTGs is,

$$\Delta \dot{\boldsymbol{Q}}_{\mathrm{W}} = \boldsymbol{A}_{\mathrm{W}}\Delta \boldsymbol{Q}_{\mathrm{W}} + \boldsymbol{B}_{\mathrm{W}}\Delta \boldsymbol{Q}_{\mathrm{W}}^{\mathrm{ref}} \tag{2}$$

where

$$\Delta \boldsymbol{Q}_{\mathrm{W}} = [\Delta Q_{\mathrm{W}_1}, \Delta Q_{\mathrm{W}_2}, \ldots, \Delta Q_{\mathrm{W}_{N_{\mathrm{W}}}}]^{\mathrm{T}},$$

$$\Delta \boldsymbol{Q}_{\mathrm{W}}^{\mathrm{ref}} = \left[\Delta Q_{\mathrm{W}_1}^{\mathrm{ref}}, \Delta Q_{\mathrm{W}_2}^{\mathrm{ref}}, \ldots, \Delta Q_{\mathrm{W}_{N_{\mathrm{W}}}}^{\mathrm{ref}}\right]^{\mathrm{T}},$$

$$\boldsymbol{A}_{\mathrm{W}} = \mathrm{diag}(-1/T_{\mathrm{W}_1}, -1/T_{\mathrm{W}_2}, \ldots, -1/T_{\mathrm{W}_{N_{\mathrm{W}}}}),$$

$$\boldsymbol{B}_{\mathrm{W}} = \mathrm{diag}(1/T_{\mathrm{W}_1}, 1/T_{\mathrm{W}_2}, \ldots, 1/T_{\mathrm{W}_{N_{\mathrm{W}}}}).$$

Full-converter WTGs (Type 4) are considered in this paper. Since the converter has voltage and current limits, the reactive power capability of WTGs varies with the actual terminal voltage V_{W} and active power output P_{W} as illustrated in Fig. 2. The active power outputs of WTGs are assumed to be constant during the prediction horizon. Hence, the Var constraints can be determined by V_{W} and Q_{W}^{0} according to the *Q*-capability curve.

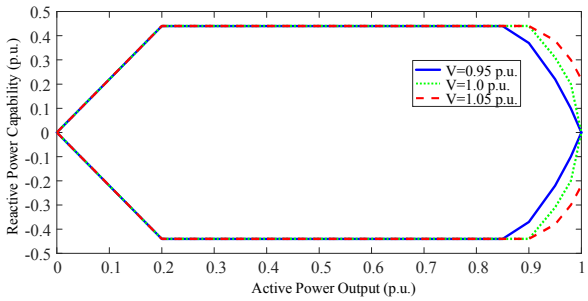

Fig. 2. *PQ curve of a full converter WTG.*

3.2. Predictive model of WPP side VSC

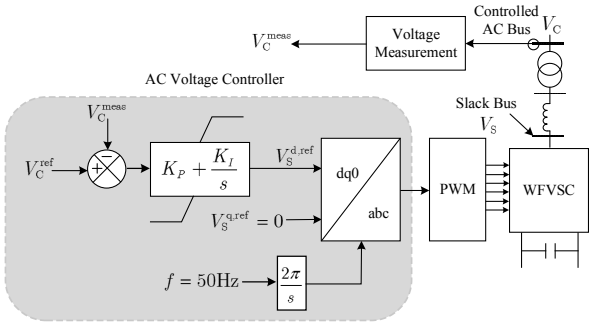

Fig. 3 *Control scheme of WPPVSC.*

As shown in Fig. 3, the offshore WPPVSC operates in the AC-voltage-control mode. The voltage of the controlled AC bus V_{C} is measured and compared with the reference value $V_{\mathrm{C}}^{\mathrm{ref}}$ from the MPC controller. The deviations between them can be eliminated by a proportional-integral (PI) controller. The voltage of the slack bus V_{S} is directly controlled by the VSC in the dynamic tracking. According to the control loop, the relationship between V_{C} and V_{S} can be described by,

$$V_{\mathrm{S}}^{\mathrm{d,ref}} = V_{\mathrm{S}}^{\mathrm{d,0}} + K_{\mathrm{p}}(V_{\mathrm{C}}^{\mathrm{ref}} - V_{\mathrm{C}}) + \frac{K_{\mathrm{i}}}{s}(V_{\mathrm{C}}^{\mathrm{ref}} - V_{\mathrm{C}}) \tag{3}$$

where K_{p} and K_{i} are the proportional and integral gains of the PI controller, respectively; $V_{\mathrm{S}}^{\mathrm{d,ref}}$ and $V_{\mathrm{S}}^{\mathrm{d,0}}$ denote reference and measured value of d-axis component of the slack bus voltage, respectively;

The PI controller provides a reference to the converter. The actual value of the voltage lags the reference due to the time-lag introduced by the PWM controller and converter's power electronics and digital control. The relation between the actual and reference values can be approximated by a time delay with time constant T_σ [20],

$$\Delta V_{\mathrm{S}}^{\mathrm{d}} = \frac{1}{1 + T_\sigma s}\Delta V_{\mathrm{S}}^{\mathrm{d,ref}} \tag{4}$$

with the following definitions,

$$\Delta V_{\mathrm{S}}^{\mathrm{d}} \triangleq V_{\mathrm{S}}^{\mathrm{d}} - V_{\mathrm{S}}^{\mathrm{d,0}},\ \Delta V_{\mathrm{S}}^{\mathrm{d,ref}} \triangleq V_{\mathrm{S}}^{\mathrm{d,ref}} - V_{\mathrm{S}}^{\mathrm{d,0}}.$$

The voltage of the controlled AC bus is affected by slack bus voltage and reactive power injections of all WTGs. Around the operating point, the system dynamics can be analyzed using a linear model,

$$V_{\mathrm{C}} = V_{\mathrm{C}}^{0} + \frac{\partial V_{\mathrm{C}}}{\partial V_{\mathrm{S}}}\Delta V_{\mathrm{S}} + \frac{\partial V_{\mathrm{C}}}{\partial \boldsymbol{Q}_{\mathrm{W}}^{\mathrm{T}}}\Delta \boldsymbol{Q}_{\mathrm{W}} \tag{5}$$

with

$$\Delta V_{\mathrm{S}} = \Delta V_{\mathrm{S}}^{\mathrm{d}},\ \Delta V_{\mathrm{S}}^{\mathrm{ref}} = \Delta V_{\mathrm{S}}^{\mathrm{d,ref}},$$

where $\partial V_{\mathrm{C}}/\partial V_{\mathrm{S}}$ and $\partial V_{\mathrm{C}}/\partial Q_{\mathrm{W}}$ are the sensitivity coefficients of V_{C} with regard to V_{S} and Q_{W}, and V_{C}^{0} is the current voltage of the controlled AC bus. As aforementioned, the active power injections of WTGs are assumed to be constant during the prediction horizon. It is because the control period in this control scheme is short (in seconds) and the variations of active power output of WTGs can be considered as unknown disturbances of the system. Moreover, the sensitivity coefficients are assumed to be constant during a prediction horizon and updated in each control period. Actually, to some degree, inaccuracies of the prediction can be compensated by the MPC. The details of sensitivity calculation are described in Section 4.

Define $\Delta V_{\mathrm{C}}^{\mathrm{ref}}$ as the reference of the voltage change and $\Delta V_{\mathrm{C}}^{\mathrm{Int}}$ as the integral of deviation between $V_{\mathrm{C}}^{\mathrm{ref}}$ and V_{C},

$$\Delta V_{\mathrm{C}}^{\mathrm{ref}} \triangleq V_{\mathrm{C}}^{\mathrm{ref}} - V_{\mathrm{C}}^{0} \tag{6}$$

$$\Delta V_{\mathrm{C}}^{\mathrm{Int}} \triangleq \frac{V_{\mathrm{C}}^{\mathrm{ref}} - V_{\mathrm{C}}}{s} = \frac{\Delta V_{\mathrm{C}}^{\mathrm{ref}} - \Delta V_{\mathrm{C}}}{s}. \tag{7}$$

Equation (3) ~ (7) are combined to obtain the predictive model of the WPPVSC,

$$\begin{bmatrix} \Delta \dot{V}_{\mathrm{S}} \\ \Delta \dot{V}_{\mathrm{C}}^{\mathrm{Int}} \end{bmatrix} = \boldsymbol{A}_{\mathrm{V}} \begin{bmatrix} \Delta V_{\mathrm{S}} \\ \Delta V_{\mathrm{C}}^{\mathrm{Int}} \end{bmatrix} + \boldsymbol{E}_{\mathrm{V}}\Delta \boldsymbol{Q}_{\mathrm{W}} + \boldsymbol{B}_{\mathrm{V}}\Delta V_{\mathrm{C}}^{\mathrm{ref}} \tag{8}$$

where

$$\boldsymbol{A}_{\mathrm{V}} = \begin{bmatrix} -\frac{1}{T_\sigma}(1 + K_{\mathrm{p}}\frac{\partial V_{\mathrm{C}}}{\partial V_{\mathrm{S}}}) & \frac{K_{\mathrm{i}}}{T_\sigma} \\ -\frac{\partial V_{\mathrm{C}}}{\partial V_{\mathrm{S}}} & 0 \end{bmatrix},\ \boldsymbol{B}_{\mathrm{V}} = \begin{bmatrix} \frac{K_{\mathrm{i}}}{T_\sigma} \\ 1 \end{bmatrix},$$

$$\boldsymbol{E}_{\mathrm{V}} = \begin{bmatrix} -\frac{K_{\mathrm{p}}}{T_\sigma}\frac{\partial V_{\mathrm{C}}}{\partial Q_{\mathrm{W}_1}} & -\frac{K_{\mathrm{p}}}{T_\sigma}\frac{\partial V_{\mathrm{C}}}{\partial Q_{\mathrm{W}_2}} & \cdots & -\frac{K_{\mathrm{p}}}{T_\sigma}\frac{\partial V_{\mathrm{C}}}{\partial Q_{\mathrm{W}_{N_{\mathrm{W}}}}} \\ -\frac{\partial V_{\mathrm{C}}}{\partial Q_{\mathrm{W}_1}} & -\frac{\partial V_{\mathrm{C}}}{\partial Q_{\mathrm{W}_2}} & \cdots & -\frac{\partial V_{\mathrm{C}}}{\partial Q_{\mathrm{W}_{N_{\mathrm{W}}}}} \end{bmatrix}.$$

The detailed derivation is presented in Appendix.

3.3. Predictive model of the system

With the developed state space models of WTGs and VSC, the state space model of the whole system including VSC and WTGs can be formulated as,

$$\dot{\boldsymbol{x}} = \boldsymbol{A}\boldsymbol{x} + \boldsymbol{B}\boldsymbol{u} \tag{9}$$

where $\boldsymbol{x}$ and $\boldsymbol{u}$ denote the state variable vector and control variable vector, which are,

$$\boldsymbol{x} = \left[\Delta V_{\mathrm{S}}, \Delta V_{\mathrm{C}}^{\mathrm{Int}}, \Delta Q_{\mathrm{W}_1}, \Delta Q_{\mathrm{W}_2}, ..., \Delta Q_{\mathrm{W}_{N_{\mathrm{W}}}}\right]^{\mathrm{T}},$$

$$\boldsymbol{u} = \left[\Delta V_{\mathrm{C}}^{\mathrm{ref}}, \Delta Q_{\mathrm{W}_1}^{\mathrm{ref}}, \Delta Q_{\mathrm{W}_2}^{\mathrm{ref}}, ..., \Delta Q_{\mathrm{W}_{N_{\mathrm{W}}}}^{\mathrm{ref}}\right]^{\mathrm{T}}.$$

And the matrixes $\boldsymbol{A}$ and $\boldsymbol{B}$ are,

$$\boldsymbol{A} = \begin{bmatrix} \boldsymbol{A}_{\mathrm{V}} & \boldsymbol{E}_{\mathrm{V}} \\ \boldsymbol{0} & \boldsymbol{A}_{\mathrm{W}} \end{bmatrix},\ \boldsymbol{B} = \begin{bmatrix} \boldsymbol{B}_{\mathrm{V}} & \boldsymbol{0} \\ \boldsymbol{0} & \boldsymbol{B}_{\mathrm{W}} \end{bmatrix}.$$

The discrete-time predictive model with sampling time ΔT_{p} can be obtained by the continuous-time model, which is,

$$\boldsymbol{x}(k+1) = \boldsymbol{G}\boldsymbol{x}(k) + \boldsymbol{H}\boldsymbol{u}(k) \tag{10}$$

where

$$\boldsymbol{G} = e^{\boldsymbol{A}\Delta T_{\mathrm{p}}},\ \boldsymbol{H} = \int_0^{\Delta T_{\mathrm{p}}} e^{\boldsymbol{A}\tau} d\tau \boldsymbol{B}.$$

4. Sensitivity calculation

Sensitivity coefficients are used to estimate the changes of objective variables in a dynamic process of MPC. In this section, the voltage magnitude sensitivities and phase angle sensitivities are calculated.

The inverse Jacobian matrix based on the Newton-Raphson formulation is commonly used for sensitivity calculation. However, such a method does not allow

computing the sensitivities against the slack bus voltage. An analytical computation method for calculating the sensitivity coefficients was developed in [20], which was initially applied in the radial distribution system.

Since the collector system in offshore WPPs has a similar configuration with radial distribution networks, the method is adopted in this paper. Compared with the numerical methods, this analytical method can be used to calculate with respect to the slack bus voltage. Moreover, it can improve the computation efficiency [20].

Considering a network comprised of N buses (N_S slack buses and N_{PQ} buses with PQ injections). $\mathcal{S}$ and $\mathcal{N}$ denote the sets of slack buses and the buses with PQ injections, respectively, i.e., $\mathcal{S} \bigcup \mathcal{N}=\{1, 2, 3,..., N\}$ with $\mathcal{S} \bigcap \mathcal{N}=\varnothing$. Define $\bar{V}_l = V_l e^{j\theta_l}$ for all buses $l \in \mathcal{S} \bigcup \mathcal{N}$ and $\bar{S}_i = P_i + \mathrm{j}Q_i$ for a bus $i \in \mathcal{N}$. The link between bus voltages and power injections is

$$\underline{S}_i = \underline{V}_i \sum_{j \in \mathcal{S} \bigcup \mathcal{N}} Y_{ij} \bar{V}_j, \qquad \forall i \in \mathcal{N} \tag{11}$$

where $\underline{V}_i$ and $\underline{S}_i$ denote the conjugates of $\bar{V}_i$ and $\bar{S}_i$, respectively; $\boldsymbol{Y} = [\bar{Y}_{ij}]_{N \times N}$ denotes the admittance matrix.

4.1. Sensitivity coefficient with respect to reactive power

To derive the voltage magnitude and phase angle sensitivity coefficients with respect to power injections, the partial derivatives of $\underline{S}_i$ with respect to reactive power Q_l of a bus $l \in \mathcal{N}$ have to be calculated, which satisfy the following equations:

$$\frac{\partial \underline{S}_i}{\partial Q_l} = \frac{\partial \{P_i - \mathrm{j}Q_i\}}{\partial Q_l} = \frac{\partial \underline{V}_i}{\partial Q_l} \sum_{j \in \mathcal{S} \bigcup \mathcal{N}} \bar{Y}_{ij} \bar{V}_j + \underline{V}_i \sum_{j \in \mathcal{N}} \bar{Y}_{ij} \frac{\partial \bar{V}_j}{\partial Q_l} = \begin{cases} -\mathrm{j}1, & \text{for } i = l. \\ 0, & \text{for } i \neq l. \end{cases} \tag{12}$$

Equation (12) is linear with $\partial \bar{V}_i / \partial Q_l$ and $\partial \underline{V}_i / \partial Q_l$. According to the theorem in [20], (12) has a unique solution for a radial network.

Once $\partial \bar{V}_i / \partial Q_l$ and $\partial \underline{V}_i / \partial Q_l$ are obtained, the voltage magnitude and phase angle sensitivity can be computed by,

$$\frac{\partial V_i}{\partial Q_l} = \frac{1}{V_i} \mathrm{Re}\left(\underline{V}_i \frac{\partial \bar{V}_i}{\partial Q_l}\right), \tag{13a}$$

$$\frac{\partial \theta_i}{\partial Q_l} = \frac{1}{V_i^2} \mathrm{Im}\left(\underline{V}_i \frac{\partial \bar{V}_i}{\partial Q_l}\right). \tag{13b}$$

4.2. Sensitivity coefficient with respect to slack bus voltage

For a bus $i \in \mathcal{N}$, the partial derivatives with respect to voltage magnitude V_k of a slack bus $k \in \mathcal{S}$ are derived by,

$$-\underline{V}_i Y_{ik} e^{j\theta_k} = \underline{W}_{ik} \sum_{j \in \mathcal{S} \bigcup \mathcal{N}} \bar{Y}_{ij} \bar{V}_j + \underline{V}_i \sum_{j \in \mathcal{N}} \bar{Y}_{ij} \bar{W}_{jk} \tag{14}$$

where

$$\bar{W}_{ik} \triangleq \frac{\partial \bar{V}_i}{\partial V_k} = \left(\frac{1}{V_i} \frac{\partial V_i}{\partial V_k} + \mathrm{j} \frac{\partial \theta_i}{\partial V_k}\right) \bar{V}_i.$$

Equation (14) is linear with respective to $\bar{W}_{ik}$ and $\underline{W}_{ik}$, and also has a unique solution. By solving it, the sensitivity coefficients with respect to the slack bus voltage magnitude at bus k are given by,

$$\frac{\partial V_i}{\partial V_k} = \frac{1}{V_i} \mathrm{Re}\left(\frac{\bar{W}_{ik}}{\bar{V}_i}\right) \tag{15a}$$

$$\frac{\partial \theta_i}{\partial V_k} = \mathrm{Im}\left(\frac{\bar{W}_{ik}}{\bar{V}_i}\right) \tag{15b}$$

5. Formulation of MPC-CVCS

For a VSC-HVDC connected offshore WPP, the offshore AC grid is decoupled from the onshore AC grid by the dc transmission system. The voltage fluctuation in the offshore AC grid cannot directly affect the voltage of the onshore POC. The main objective of the offshore WPP voltage control is to maintain terminal voltages of all WTGs within specified limits. In addition, the economical operation of offshore WPPs should also be considered. To coordinate the economical operation and voltage control, two control modes with different control objectives are designed for different operating conditions. In the optimization operation mode, several key bus voltages in offshore WPPs, power losses, and Var reserves are coordinated. Most of the time, the system operates in this mode. The corrective mode is a back-up mode in the MPC-CVCS which aims to correct the WTGs' terminal voltages.

To capture the dynamic characteristics of different devices, the sampling period of prediction ΔT_P should be much smaller than the period of control action T_C, which is normally in seconds. The suitable prediction horizon T_P can be determined by the performance of the control system. Too large or too small prediction horizon will adversely affect the control performance. Accordingly, for o prediction horizon, the total number of prediction steps and control steps are calculated by $N_P = T_P / \Delta T_P$ and $N_C = T_P / T_C$, respectively.

5.1. Optimization operation mode

If all WTG terminal voltages in the offshore grid are within the feasible range，i.e., $\|V_W - V_W^{ref}\| < V_W^{th}$, where V_W^{th} is the threshold value, the MPC controller will operate in the optimization operation mode. V_W^{ref} is the nominal terminal voltage of each WTG (typically 1.0 p.u.). Since the limits are generally set as [0.9,1.1] p.u., V_W^{th} can be selected as 0.05 ~ 0.08 p.u. in implementation to ensure sufficient operation margins.

The power losses and Var reserves are both optimized in this mode. In the meantime, to maintain the system voltage within the limits, voltages of several important buses shall also be taken into account.

1) Objective 1: The first objective is to minimize the bus voltage deviations in the offshore AC grid. Generally, each offshore WPP comprised of several radial feeders can be considered as an isolate voltage regulation sub-zone. For each radial medium-voltage (MV) feeder, the root bus which is the center of the subzone from the point view of electrical distance can be regarded as the pilot bus of the sub-zone [21]. It means that the voltage conditions of the sub-zones can be reflected by the MV buses. In other words, to simplify the control objective, only the voltages of pilot buses are controlled. Defining $\Delta V_{MV} \triangleq V_{MV} - V_{MV}^{ref}$, the cost function OBJ_V can be described by,

$$\mathrm{OBJ_V}=\sum_{k=1}^{N_\mathrm{P}}\left\|\Delta \boldsymbol{V}_{\mathrm{MV}}^{\mathrm{pre}}(k)\right\|^2 \tag{16}$$

where $\Delta \boldsymbol{V}_{\mathrm{MV}}=[\Delta V_{\mathrm{MV}_1},\Delta V_{\mathrm{MV}_2},...,\Delta V_{\mathrm{MV}_{N_\mathrm{MV}}}]^{\mathrm{T}}$, and N_{MV} is the number of MV buses.

ΔV_{MV} can be affected by control actions of VSC and reactive power outputs of WTGs. The predictive value of ΔV_{MV} can be calculated by,

$$\Delta V_{\mathrm{MV}}^{\mathrm{pre}}(k)=V_{\mathrm{MV}}^{0}+\frac{\partial V_{\mathrm{MV}}}{\partial V_{\mathrm{S}}}\Delta V_{\mathrm{S}}(k)+\frac{\partial V_{\mathrm{MV}}}{\partial \boldsymbol{Q}_{\mathrm{W}}^{\mathrm{T}}}\Delta \boldsymbol{Q}_{\mathrm{W}}(k)-V_{\mathrm{MV}}^{\mathrm{ref}} \tag{17}$$

where V_{MV}^{0} and $V_{\mathrm{MV}}^{\mathrm{ref}}$ are the current value and nominal value (typically 1.0 p.u.) of V_{MV}, respectively.

2) Objective 2: The second control objective is to minimize the active power losses P_{L} inside the offshore AC grid, which depend on the power flow distribution of the grid. The cost function $\mathrm{OBJ_L}$ can be described as,

$$\mathrm{OBJ_L}=\sum_{k=1}^{N_\mathrm{P}}\left\|P_{\mathrm{L}}^{\mathrm{pre}}(k)\right\|^2. \tag{18}$$

Defining

$$\boldsymbol{V}\triangleq[V_1,V_2,...,V_N]^{\mathrm{T}},\ \boldsymbol{\theta}\triangleq[\theta_1,\theta_2,...,\theta_N]^{\mathrm{T}},$$

the predictive value of power losses $P_{\mathrm{L}}^{\mathrm{pre}}$ can be calculated by,

$$\begin{aligned}P_{\mathrm{L}}^{\mathrm{pre}}(k)=P_{\mathrm{L}}^{0}&+\left(\frac{\partial P_{\mathrm{L}}}{\partial \boldsymbol{V}^{\mathrm{T}}}\frac{\partial \boldsymbol{V}}{\partial V_{\mathrm{S}}}+\frac{\partial P_{\mathrm{L}}}{\partial \boldsymbol{\theta}^{\mathrm{T}}}\frac{\partial \boldsymbol{\theta}}{\partial V_{\mathrm{S}}}\right)\Delta V_{\mathrm{S}}(k)\\&+\left(\frac{\partial P_{\mathrm{L}}}{\partial \boldsymbol{V}^{\mathrm{T}}}\frac{\partial \boldsymbol{V}}{\partial \boldsymbol{Q}_{\mathrm{W}}^{\mathrm{T}}}+\frac{\partial P_{\mathrm{L}}}{\partial \boldsymbol{\theta}^{\mathrm{T}}}\frac{\partial \boldsymbol{\theta}}{\partial \boldsymbol{Q}_{\mathrm{W}}^{\mathrm{T}}}\right)\Delta \boldsymbol{Q}_{\mathrm{W}}(k)\end{aligned} \tag{19}$$

with

$$\frac{\partial P_{\mathrm{L}}}{\partial V_i}=2\sum_{j=1}^{N}V_jG_{ji}\cos(\theta_j-\theta_i),$$

$$\frac{\partial P_{\mathrm{L}}}{\partial \theta_i}=2\sum_{j=1}^{N}V_iV_jG_{ji}\sin(\theta_j-\theta_i).$$

where G_{ij} is the real part of the admittance matrix.

3) Objective 3: The third objective is to maximize the Var reserves of WTGs. The cost function $\mathrm{OBJ_Q}$ is expressed as,

$$\mathrm{OBJ_Q}=\sum_{k=1}^{N_\mathrm{P}}\left\|\Delta \boldsymbol{Q}_{\mathrm{W,DEV}}^{\mathrm{pre}}(k)\right\|^2 \tag{20}$$

where $\Delta Q_{\mathrm{W,DEV}}^{\mathrm{pre}}(k)$ is the predictive deviation of Q_{W} from its middle operating level, which can be calculated by,

$$\Delta Q_{\mathrm{W,DEV}}^{\mathrm{pre}}(k)=Q_{\mathrm{W}}^{0}+\Delta Q_{\mathrm{W}}(k)-\frac{1}{2}(Q_{\mathrm{W}}^{\max}+Q_{\mathrm{W}}^{\min}) \tag{21}$$

where $Q_{\mathrm{W}}^{\max}$ and $Q_{\mathrm{W}}^{\min}$ are the Var limits of WTGs.

Combining (16), (18) and (20), the mathematical model of this mode is as follows,

$$\min_{\Delta V_{\mathrm{C}}^{\mathrm{ref}},\ \Delta \boldsymbol{Q}_{\mathrm{W}}^{\mathrm{ref}}}\ (w_{\mathrm{V}}\cdot\mathrm{OBJ_V}+w_{\mathrm{L}}\cdot\mathrm{OBJ_L}+w_{\mathrm{Q}}\cdot\mathrm{OBJ_Q})$$

subject to

$$\begin{aligned}&V_{\mathrm{C}}^{\min}\le V_{\mathrm{C}}^{0}+\Delta V_{\mathrm{C}}^{\mathrm{ref}}(n)\le V_{\mathrm{C}}^{\max},\\&\left|\Delta V_{\mathrm{C}}^{\mathrm{ref}}(n)-\Delta V_{\mathrm{C}}^{\mathrm{ref}}(n-1)\right|<\Delta V_{\mathrm{C}}^{\max},\\&Q_{\mathrm{W}}^{\min}\le \boldsymbol{Q}_{\mathrm{W}}^{0}+\Delta \boldsymbol{Q}_{\mathrm{W}}(k)\le Q_{\mathrm{W}}^{\max},\\&V_{\mathrm{MV}}^{\min}\le \boldsymbol{V}_{\mathrm{MV}}^{0}+\Delta \boldsymbol{V}_{\mathrm{MV}}^{\mathrm{pre}}(k)\le V_{\mathrm{MV}}^{\max},\\&n=1,2,...,N_{\mathrm{C}},\quad k=1,2,...,N_{\mathrm{P}}.\end{aligned} \tag{22}$$

where $V_{\mathrm{MV}}^{\min}$, $V_{\mathrm{MV}}^{\max}$, $V_{\mathrm{C}}^{\min}$, $V_{\mathrm{C}}^{\max}$ and $\Delta V_{\mathrm{C}}^{\max}$ are the operating limits of V_{MV} and V_{C}, and w_{V}, w_{L} and w_{Q} are the weighting coefficients which depend on the control priority determined by the operators. The priority ranking is $\mathrm{OBJ_L}>\mathrm{OBJ_Q}>\mathrm{OBJ_V}$ in this study.

5.2. Corrective mode

The corrective mode is a back-up mode for voltage regulation. If any WTG terminal bus voltage violates the threshold, the control mode will switch into the corrective mode, and the control objective will change to voltage correction. In this mode, the terminal voltages of WTGs are corrected. Defining $\Delta V_{\mathrm{W}}\triangleq V_{\mathrm{W}}-V_{\mathrm{W}}^{\mathrm{ref}}$, the mathematical model of this mode is as follows,

$$\min_{\Delta V_{\mathrm{C}}^{\mathrm{ref}},\ \Delta \boldsymbol{Q}_{\mathrm{W}}^{\mathrm{ref}}}\ \sum_{k=1}^{N_\mathrm{P}}\left\|\Delta \boldsymbol{V}_{\mathrm{W}}^{\mathrm{pre}}(k)\right\|_{\boldsymbol{w}}^2$$

subject to

$$\begin{aligned}&V_{\mathrm{C}}^{\min}\le V_{\mathrm{C}}^{0}+\Delta V_{\mathrm{C}}^{\mathrm{ref}}(n)\le V_{\mathrm{C}}^{\max},\\&|\Delta V_{\mathrm{C}}^{\mathrm{ref}}(n)-\Delta V_{\mathrm{C}}^{\mathrm{ref}}(n-1)|<\Delta V_{\mathrm{C}}^{\max},\\&Q_{\mathrm{W}}^{\min}\le \boldsymbol{Q}_{\mathrm{W}}^{0}+\Delta \boldsymbol{Q}_{\mathrm{W}}(k)\le Q_{\mathrm{W}}^{\max},\\&n=1,2,...,N_{\mathrm{C}},\quad k=1,2,...,N_{\mathrm{P}}.\end{aligned} \tag{23}$$

where $\boldsymbol{w}=\mathrm{diag}(w_{\mathrm{W}_1},w_{\mathrm{W}_2},...,w_{\mathrm{W}_{N_\mathrm{W}}})$ is the weight coefficient matrix, and $\Delta \boldsymbol{V}_{\mathrm{W}}^{\mathrm{pre}}=[\Delta V_{\mathrm{W}_1}^{\mathrm{pre}},\Delta V_{\mathrm{W}_2}^{\mathrm{pre}},...,\Delta V_{\mathrm{W}_{N_\mathrm{W}}}^{\mathrm{pre}}]^{\mathrm{T}}$ denotes the vector of predictive voltage deviation which can be calculated by,

$$\Delta V_{\mathrm{W}}^{\mathrm{pre}}(k)=V_{\mathrm{W}}^{0}+\frac{\partial V_{\mathrm{W}}}{\partial V_{\mathrm{S}}}\Delta V_{\mathrm{S}}(k)+\frac{\partial V_{\mathrm{W}}}{\partial \boldsymbol{Q}_{\mathrm{W}}^{\mathrm{T}}}\Delta \boldsymbol{Q}_{\mathrm{W}}(k)-V_{\mathrm{W}}^{\mathrm{ref}}. \tag{24}$$

To correct the voltages more efficiently, the dynamic adaptive weighting coefficients are used for this mode. An adaptive weighting coefficient calculation method is illustrated in Fig. 4. To correct the voltages of high-risk buses, a dead-band for voltage deviation with a threshold of ±0.02 p.u. is designed in this mode.

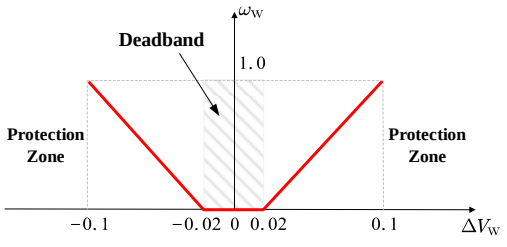

Fig. 4. *Adaptive weighting coefficients.*

The developed mathematical optimization models of the MPC-CVCS can be transformed into a standard quadratic programming (QP) problem, and be efficiently solved by a QP solver.

6. Simulation results

6.1. System configuration and parameters

A typical configuration of an offshore WPP is illustrated in Fig. 5. The offshore WPP comprised of two parts is connected to the onshore external 400 kV AC grid through a ±150 kV VSC-HVDC system with nominal power rating of 400 MW. Each part is equipped with a collector substation, and the substations are connected to a common VSC station through 150 kV submarine cables. The WTGs are connected by eight 33 kV collector cables. MV bus_1~MV bus_4 are considered as the pilot buses of each subzone. There are eight full-converter 6.25 MW WTGs at each feeder, referred to as a string. The WTGs are placed with a distance of 1.5 km. The system parameters are presented in Table I. The wind field model considering turbulences and wake effects for the offshore WPP is generated using SimWindFarm [22], a toolbox for wind farm modeling and simulation.

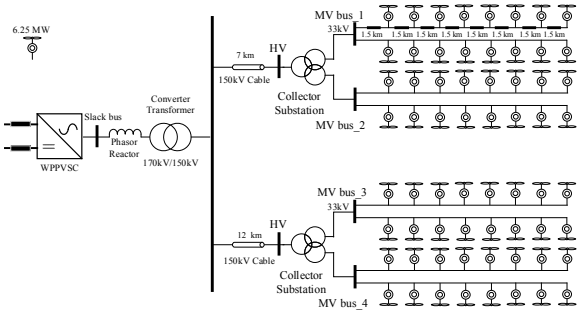

Fig. 5. *Configuration of a VSC-HVDC connected offshore WPP.*

Table 1 Electrical system parameters

Parameters	Value
33kV Cable	R=0.0975 Ω/km, L=0.38 mH/km, C=0.24 μF/km
150kV Cable	R=0.0326 Ω/km, L=0.42 mH/km, C=0.15 μF/km
33/150kV Transformer	S_n = 100 MVA , R=0.005 p.u., X=0.12 p.u.
150/170kV Transformer	S_n = 400 MVA , R=0.006 p.u., X=0.14 p.u.
Phasor Reactor	0.0178 + j 0.196 p.u.

To examine the performance of the proposed MPC-CVCS, two other control methods are simulated and compared with the MPC-based method.

1) Loss Minimization Control (LMC). For the LMC, the control actions are determined by the optimal power flow analysis which aims to minimize power losses in the grid.

2) Optimal Control (OPC) [10]. For the OPC, the objective is to minimize the cost function of current stage without considering the effects on the future (without considering the dynamic response of the system).

The control period T_C , prediction horizon T_P and sampling period of prediction ΔT_P are set as 1 s, 5 s, and 0.1 s, respectively. The feasible range of V_C^{ref} is set as [0.99, 1.01] p.u.. The threshold V_W^{th} is set as 0.05 p.u.. The OPC and LMC have the same control period as the MPC. Besides, the OPC also has two control modes with the same threshold values as the MPC.

6.2. Normal Operation

The performance of the proposed voltage control scheme is validated with fluctuating wind power. The total simulation time is set as 600 s. As shown in Fig. 6, the total wind power of the offshore WPP fluctuates between 220 MW to 380MW during the simulation. The voltages, Var reserves of WTGs and power losses are analyzed, which are shown in Fig. 7.

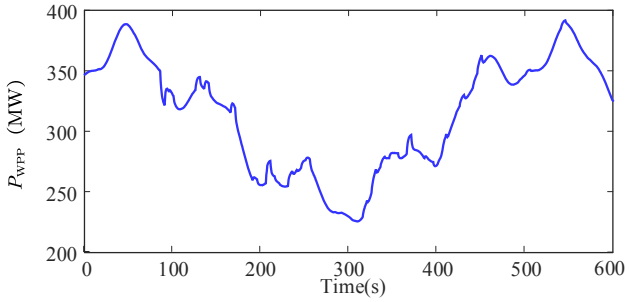

Fig. 6. *Power output of the offshore WPP.*

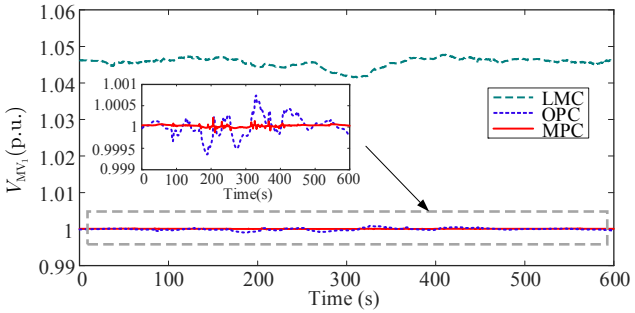

a

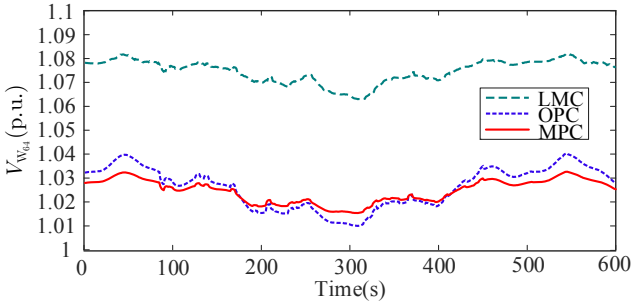

b

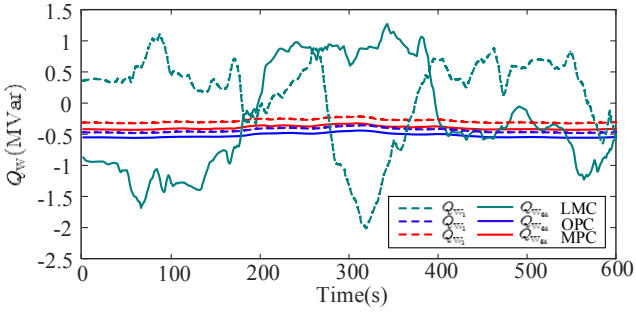

c

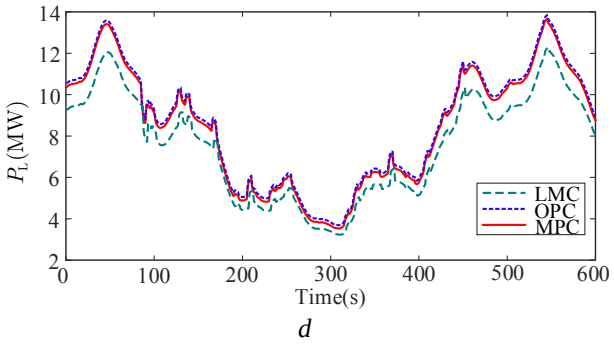

d

Fig. 7. *Voltages, Var reserves of WTGs and active power losses under normal operation.* **(a)** Voltage of MV bus_1; **(b)** Terminal voltage of WTG_64. **(c)** Reactive power outputs of WTG_1 and WTG_64. **(d)** Active power losses.

The simulation results of MV bus_1 voltage are shown in Fig. 7*a*. It can be seen the MPC and OPC can both regulate it around its reference value 1.0 p.u. with slight deviations and the voltage fluctuations are small. However, the LMC cannot efficiently regulate the voltage. The mean values of the voltage are 1.0472 p.u., 1.0000 p.u. and 1.0001 p.u., and the standard deviations are 0.1326%, 0.0185% and 0.0027% for LMC, OPC and MPC, respectively.

The furthest bus of a feeder has the highest risk of overvoltage. The terminal of WTG_64 is selected as the representative bus, and the simulation results are shown in Fig. 7*b*. Similarly, the MPC and OPC show better performance on voltage regulation. The terminal voltage of WTG_64 is quite close to the upper limit of the feasible range regulated by LMC controller. The standard deviations of the voltage are 0.4775%, 0.4841% and 0.3762% for the LMC, OPC and MPC, respectively.

Fig. 7*c* shows the reactive power outputs of two WTGs (WTG_1 and WTG_64). The LMC regulated reactive power outputs fluctuate the most among the three methods because it only minimizes the power losses. Most of the time, the Var reserves of WTGs are quite small. The OPC and MPC can both regulate the reactive power outputs within small ranges, which means there are bigger Var reserves to deal with the potential disturbance in this future. For the MPC, the mean values of reactive power outputs of WTG_1 and WTG_64 are -0.35 MW and -0.4 MW, respectively. For the OPC, they are -0.44 MW and -0.52 MW, respectively. Therefore, the Var reserve with the MPC is bigger than that with the OPC.

Fig. 7*d* shows power losses of the offshore AC grid. The LMC performs better in power losses reduction with the mean value of 7.5934 MW. The mean values of power losses are 8.4964 MW and 8.4028 MW for the OPC and MPC. Compared with the OPC, the MPC is better. Considering the overall performance, the MPC performs better than the OPC and LMC.

6.3. Recovery Operation

In this case, the recovery operation of the offshore WPP after a storm is considered. The WPPVSC gradually builds up the voltage at the beginning. When the terminal voltages of WTGs reach 0.9 p.u., WTGs are connected to the grid and the voltage control strategy switches to the proposed coordinated voltage control strategy. The recovery operation starts at $t = 20$ s . The total simulation time is 50 s. The simulation results are shown in Fig. 8. The control strategy switches to the coordinated control strategy at $t = 28$ s .

As shown in Fig. 8, for the OPC, the terminal voltage of WTG_64 returns within its threshold (0.95 p.u.) at $t = 28.8$ s and reaches its reference (1.0 p.u.) at $t = 31.3$ s . The MV bus_1 voltage reaches its reference (1.0 p.u.) at $t = 33.4$ s .

For the MPC, the voltage recovery is faster. The terminal voltage of WTG_64 returns within its threshold at $t = 28.4$ s and reaches 1.0 p.u. at $t = 29.4$ s . The MV bus_1 voltage reaches 1.0 p.u. at $t = 29.6$ s . The MPC performs better than the OPC in the recovery operation.

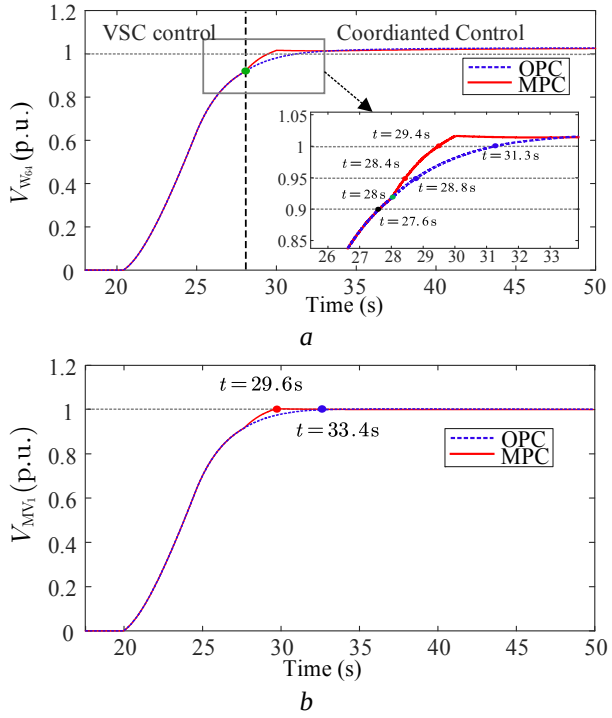

a

b

Fig. 8. *Bus voltages under recovery operation.* **(a)** Terminal voltage of WTG_64;**(b)** Voltage of MV Bus_1

6.4. Robust test

This subsection is concerned with the robustness of the proposed controller to communication time delay and measurement errors.

6.4.1 Communication delay

The impact of different communication time delay should be considered in voltage controller design. Fig. 9*a* shows the voltage of MV bus_1 with the communication time delay of 0 ms, 100ms and 200 ms, respectively. Fig. 9*b* shows the reactive power output of WTG_64. As can be seen, with the increase of time delay, the voltage of MV bus_1 and the reactive power output of WTG_64 fluctuate within a slightly larger range, however, the system is still fully stable. The communication delay has slight effect in normal operation.

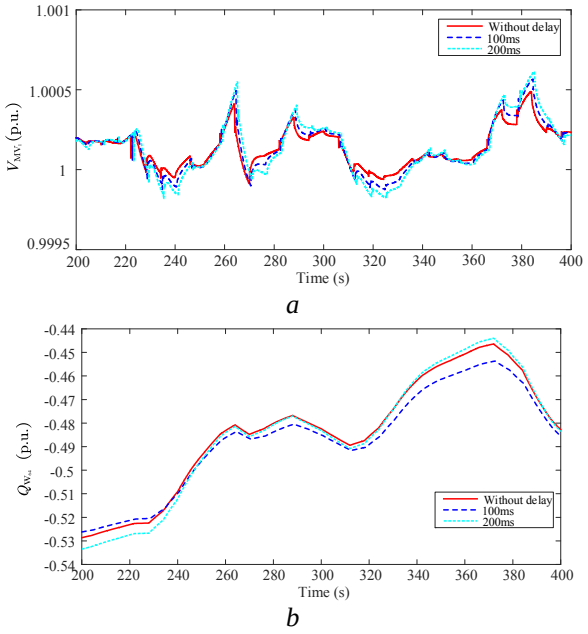

Fig. 9. *Control performance with different communication time delay.* **(a)** Voltage of MV bus_1; **(b)** reactive power output of WTG_64.

6.4.1 Measurement errors

Here, the control performance of the proposed voltage controller with different measurement errors is compared. Suppose the stochastic measurement error ε follows normal distribution with the same mean and variance for all buses. Thus, the measured voltage magnitude received by the controller can be expressed as,

$$\tilde{V} = (1+\varepsilon)\cdot V, \quad \varepsilon \sim N(0,\sigma^2). \tag{25}$$

The variance σ is set as 2% and 5%, respectively.

Fig. 10 shows the effect of measurement errors on the voltage of MV bus_1. The voltage is significantly affected by the measurement errors. Increasing the level of measurement errors deteriorates the control performance. But the voltage can be still regulated within the acceptable range of 0.99~1.01 p.u. and the system is still stable.

From the analysis of this subsection, we can conclude that the controller shows satisfactory robustness to these uncertain factors.

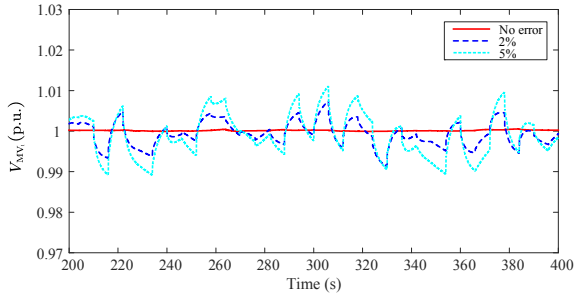

Fig. 10. *Voltage of MV bus_1 under different measurement errors.*

7. Conclusion

A MPC-CVCS for VSC-HVDC connected offshore WPPs is proposed to coordinate voltage control and economical control in offshore AC grid. In the proposed MPC-CVCS, the flexibility of VSC in voltage regulation is utilized. Two control modes are designed for the coordination of economical operation and voltage stability. The superior performance of the proposed MPC-CVCS is demonstrated by comparing it to the OPC and LMC. Though communication time delay and measurement errors can deteriorate control performance, the controller can still effectively regulate the voltage within the feasible range and keep the system stable.

8. Appendix

8.1. Derivation of predictive model of WPPVSC

The derivation of the predictive model of WPPVSC is presented in this section.

Substitute (5), (6) and (7) into (3), (3) can be transformed into,

$$\Delta V_{\mathrm{S}}^{\mathrm{ref}} = K_{\mathrm{p}}\left(\Delta V_{\mathrm{C}}^{\mathrm{ref}} - \frac{\partial V_{\mathrm{C}}}{\partial V_{\mathrm{S}}}\Delta V_{S} - \frac{\partial V_{\mathrm{C}}}{\partial \boldsymbol{Q}_{\mathrm{W}}^{\mathrm{T}}}\Delta \boldsymbol{Q}_{\mathrm{W}}\right) + K_{\mathrm{i}}\Delta V_{\mathrm{C}}^{\mathrm{Int}}. \tag{26}$$

The equation (4) can be transformed into,

$$\Delta \dot{V}_{\mathrm{S}} = -\frac{1}{T_\sigma}\Delta V_{\mathrm{S}} + \frac{1}{T_\sigma}\Delta V_{\mathrm{S}}^{\mathrm{ref}}. \tag{27}$$

Substitute (26) into (27),

$$\begin{aligned}\Delta \dot{V}_{\mathrm{S}} = &-\frac{1}{T_\sigma}\left(1+K_{\mathrm{p}}\frac{\partial V_{\mathrm{C}}}{\partial V_{\mathrm{S}}}\right)\Delta V_{\mathrm{S}} + \frac{K_{\mathrm{i}}}{T_\sigma}V_{\mathrm{C}}^{\mathrm{Int}} \\ &-\frac{K_{\mathrm{p}}}{T_\sigma}\frac{\partial V_{\mathrm{C}}}{\partial \boldsymbol{Q}_{\mathrm{W}}^{\mathrm{T}}}\Delta \boldsymbol{Q}_{\mathrm{W}} + \frac{K_{\mathrm{p}}}{T_\sigma}\Delta V_{\mathrm{C}}^{\mathrm{ref}}\end{aligned} \tag{28}$$

The equation (7) can be rewritten as

$$\Delta \dot{V}_{\mathrm{C}}^{\mathrm{Int}} = \Delta V_{\mathrm{C}}^{\mathrm{ref}} - \Delta V_{\mathrm{C}}. \tag{29}$$

Substitute (5) and (6) into (29),

$$\Delta \dot{V}_{\mathrm{C}}^{\mathrm{Int}} = -\frac{\partial V_{\mathrm{C}}}{\partial V_{\mathrm{S}}}\Delta V_{\mathrm{S}} - \frac{\partial V_{\mathrm{C}}}{\partial \boldsymbol{Q}_{\mathrm{W}}^{\mathrm{T}}}\Delta \boldsymbol{Q}_{\mathrm{W}} + \Delta V_{\mathrm{C}}^{\mathrm{ref}} \tag{30}$$

Rewrite (29) and (31) into a matrix form, and then the corresponding matrixes in the predictive model are,

$$\boldsymbol{A}_{\mathrm{V}} = \begin{bmatrix} -\frac{1}{T_\sigma}\left(1+K_{\mathrm{p}}\frac{\partial V_{\mathrm{C}}}{\partial V_{\mathrm{S}}}\right) & \frac{K_{\mathrm{i}}}{T_\sigma} \\ -\frac{\partial V_{\mathrm{C}}}{\partial V_{\mathrm{S}}} & 0 \end{bmatrix},\ \boldsymbol{B}_{\mathrm{V}} = \begin{bmatrix} \frac{K_{\mathrm{i}}}{T_\sigma} \\ 1 \end{bmatrix},$$

$$\boldsymbol{E}_{\mathrm{V}} = \begin{bmatrix} -\frac{K_{\mathrm{p}}}{T_\sigma}\frac{\partial V_{\mathrm{C}}}{\partial Q_{\mathrm{W}_1}} & -\frac{K_{\mathrm{p}}}{T_\sigma}\frac{\partial V_{\mathrm{C}}}{\partial Q_{\mathrm{W}_2}} & \cdots & -\frac{K_{\mathrm{p}}}{T_\sigma}\frac{\partial V_{\mathrm{C}}}{\partial Q_{\mathrm{W}_{N_{\mathrm{W}}}}} \\ -\frac{\partial V_{\mathrm{C}}}{\partial Q_{\mathrm{W}_1}} & -\frac{\partial V_{\mathrm{C}}}{\partial Q_{\mathrm{W}_2}} & \cdots & -\frac{\partial V_{\mathrm{C}}}{\partial Q_{\mathrm{W}_{N_{\mathrm{W}}}}} \end{bmatrix}. \tag{31}$$

8.2. Derivation of sensitivity coefficient calculation

The derivations of sensitivity coefficients ($\partial V_i / \partial Q_l$, $\partial \theta_i / \partial Q_l$) and ($\partial V_i / \partial V_k$, $\partial \theta_i / \partial V_k$) are similar. So, due the page limit, only the derivation of ($\partial V_i / \partial Q_l$, $\partial \theta_i / \partial Q_l$) is presented in this paper. The derivation can be divided into two steps.

Step I: Calculation of $\partial \overline{V}_i / \partial Q_l$ and $\partial \underline{V}_j / \partial Q_l$.

The derivation starts from (11). Firstly, by taking the derivatives with respective reactive power injections, we can obtain (12). Firstly, define

$$\frac{\partial \overline{V}_i}{\partial Q_l} \triangleq x_{il} + \mathrm{j}\, y_{il}, \tag{32}$$

$$\sum_{j\in\mathcal{S}\cup\mathcal{N}} \overline{Y}_{ij}\overline{V}_j \triangleq w_{i1} + \mathrm{j}w_{i2}, \tag{33}$$

$$\underline{V}_i\overline{Y}_{ij} \triangleq a_{ij} + \mathrm{j}b_{ij}. \tag{34}$$

Obviously, (33) and (34) can be calculated according to measured voltage. The unknown variables are x_{il} and y_{il}. Substitute (32)-(34) into (12), it can be obtained that,

$$\begin{aligned}
\frac{\partial \underline{S}_i}{\partial Q_l} &= \frac{\partial \underline{V}_i}{\partial Q_l}\sum_{j\in\mathcal{S}\cup\mathcal{N}} \overline{Y}_{ij}\overline{V}_j + \underline{V}_i\sum_{j\in\mathcal{N}} \overline{Y}_{ij}\frac{\partial \overline{V}_j}{\partial Q_l} \\
&= (x_{il} - \mathrm{j}y_{il})(w_{i1} + \mathrm{j}w_{i2}) + \sum_{j\in\mathcal{N}}(a_{ij} + \mathrm{j}b_{ij})(x_{jl} + \mathrm{j}y_{jl}) \\
&= (x_{il} - \mathrm{j}y_{il})(w_{i1} + \mathrm{j}w_{i2}) + (a_{i1} + \mathrm{j}b_{i1})(x_{1l} + \mathrm{j}y_{1l}) \\
&+(a_{i2} + \mathrm{j}b_{i2})(x_{2l} + \mathrm{j}y_{2l}) + \cdots + (a_{i,N_{PQ}} + \mathrm{j}b_{i,N_{PQ}})(x_{N_{PQ},l} + \mathrm{j}y_{N_{PQ},l}) \\
&= (w_{i1}x_{il} + w_{i2}y_{il}) + \mathrm{j}(w_{i2}x_{il} - w_{i1}y_{il}) + (a_{i1}x_{1l} - b_{i1}y_{1l}) \\
&+ \mathrm{j}(a_{i1}y_{1l} + b_{i1}x_{1l}) + (a_{i2}x_{2l} - b_{21}y_{2l}) + \mathrm{j}(a_{i2}y_{2l} + b_{i2}x_{2l}) \\
&+\cdots + (a_{i,N_{PQ}}x_{N_{PQ},l} - b_{i,N_{PQ}}y_{N_{PQ},l}) + \mathrm{j}(a_{i,N_{PQ}}y_{N_{PQ},l} + b_{i,N_{PQ}}x_{N_{PQ},l}).
\end{aligned} \tag{35}$$

Rearrange (35) and then the real part and imaginary part of (35) are separately expressed as:

Real Part:

$$\begin{aligned}
&(w_{i1}x_{il} + w_{i2}y_{il}) + (a_{i1}x_{1l} - b_{i1}y_{1l}) + (a_{i2}x_{2l} - b_{21}y_{2l}) \\
&\qquad +\cdots + (a_{i,N_{PQ}}x_{N_{PQ},l} - b_{i,N_{PQ}}y_{N_{PQ},l}) = 0
\end{aligned}, \tag{36}$$

Imaginary Part:

$$\begin{aligned}
&(w_{i2}x_{il} - w_{i1}y_{il}) + (a_{i1}y_{1l} + b_{i1}x_{1l}) + (a_{i2}y_{2l} + b_{i2}x_{2l}) \\
&\qquad +\cdots + (a_{i,N_{PQ}}y_{N_{PQ},l} + b_{i,N_{PQ}}x_{N_{PQ},l}) = \begin{cases} -1, & \text{for } i = l. \\ 0, & \text{for } i \neq l. \end{cases}
\end{aligned} \tag{37}$$

So, for any bus $l \in \mathcal{N}$, by formulating (36) and (37) for all $i \in \mathcal{N}$, a set of equation can be formulated into a matrix form as follows:

$$(\boldsymbol{C}_1 + \boldsymbol{C}_2)\boldsymbol{z} = \boldsymbol{d}, \tag{38}$$

where

$$\boldsymbol{C}_1 = \begin{bmatrix}
a_{11} & -b_{11} & a_{12} & -b_{12} & \cdots & a_{1,N_{PQ}} & -b_{1,N_{PQ}} \\
b_{11} & a_{11} & b_{12} & a_{12} & \cdots & b_{1,N_{PQ}} & a_{1,N_{PQ}} \\
\vdots & \vdots & \vdots & \vdots & \vdots & \vdots & \vdots \\
a_{i1} & -b_{i1} & a_{i2} & -b_{i2} & \cdots & a_{i,N_{PQ}} & -b_{i,N_{PQ}} \\
b_{i1} & a_{i1} & b_{i2} & a_{i2} & \cdots & b_{i,N_{PQ}} & a_{i,N_{PQ}} \\
\vdots & \vdots & \vdots & \vdots & \vdots & \vdots & \vdots \\
a_{i,N_{PQ}} & -b_{i,N_{PQ}} & a_{i,N_{PQ}} & -b_{i,N_{PQ}} & \cdots & a_{i,N_{PQ}} & -b_{i,N_{PQ}} \\
b_{i,N_{PQ}} & a_{i,N_{PQ}} & b_{i,N_{PQ}} & a_{i,N_{PQ}} & \cdots & b_{i,N_{PQ}} & a_{i,N_{PQ}}
\end{bmatrix}$$

$$\boldsymbol{C}_2 = \begin{bmatrix}
w_{11} & w_{12} & 0 & 0 & \cdots & 0 & 0 \\
w_{12} & -w_{11} & 0 & 0 & \cdots & 0 & 0 \\
0 & 0 & w_{21} & w_{22} & \cdots & 0 & 0 \\
0 & 0 & w_{22} & -w_{21} & \cdots & 0 & 0 \\
\vdots & \vdots & \vdots & \vdots & \ddots & \vdots & \vdots \\
0 & 0 & 0 & 0 & \cdots & w_{N_{PQ},1} & w_{N_{PQ},2} \\
0 & 0 & 0 & 0 & \cdots & w_{N_{PQ},2} & -w_{N_{PQ},1}
\end{bmatrix},$$

$$\boldsymbol{z} = [x_{1l}, y_{1l}, x_{2l}, y_{2l}, \ldots, x_{N_{PQ},l}, y_{N_{PQ},l}]^T,$$

$$\boldsymbol{d} = [\underbrace{0,0,0,0,\ldots,}_{2\times(l-1)}0,-1,\ldots,0,0]^T.$$

Then, the pending sensitivity coefficients $\partial\overline{V}_i / \partial Q_l$ and $\partial\underline{V}_i / \partial Q_l$ can be obtained by,

$$\boldsymbol{z} = (\boldsymbol{C}_1 + \boldsymbol{C}_2)^{-1}\boldsymbol{d}. \tag{39}$$

Step II: Calculation of $\partial V_i / \partial Q_l$ and $\partial\theta_i / \partial Q_l$.

Define $\overline{V}_i \triangleq V_i\angle\theta_i = V_i(\cos\theta_i + \mathrm{j}\sin\theta_i)$, then

$$\begin{aligned}
\underline{V}_i\frac{\partial \overline{V}_i}{\partial Q_l} &= V_i(\cos\theta_i - \mathrm{j}\sin\theta_i)\cdot\frac{\partial\{V_i\cos\theta_i + \mathrm{j}\,V_i\sin\theta_i\}}{\partial Q_l} \\
&= \left(V_i\cos\theta_i\frac{\partial\{V_i\cos\theta_i\}}{\partial Q_l} + V_i\sin\theta_i\frac{\partial\{V_i\sin\theta_i\}}{\partial Q_l}\right) \\
&\quad + \mathrm{j}\left(V_i\cos\theta_i\frac{\partial\{V_i\sin\theta_i\}}{\partial Q_l} - V_i\sin\theta_i\frac{\partial\{V_i\cos\theta_i\}}{\partial Q_l}\right)
\end{aligned} \tag{40}$$

According to

$$\frac{\partial V_i^2}{\partial Q_l} = 2V_i\frac{\partial V_i}{\partial Q_l}, \tag{41}$$

it can be obtained that

$$\begin{aligned}
\frac{\partial V_i}{\partial Q_l} &= \frac{1}{2V_i}\frac{\partial(\overline{V}_i\cdot\underline{V}_i)}{\partial Q_l} = \frac{1}{2V_i}\cdot\left(\frac{\partial\overline{V}_i}{\partial Q_l}\underline{V}_i + \frac{\partial\underline{V}_i}{\partial Q_l}\overline{V}_i\right) \\
&= \frac{1}{2V_i}\Big(\frac{\partial\{V_i\cos\theta_i + \mathrm{j}\,V_i\sin\theta_i\}}{\partial Q_l}(V_i\cos\theta_i - \mathrm{j}\,V_i\sin\theta) \\
&\quad + \frac{\partial\{V_i\cos\theta_i - \mathrm{j}\,V_i\sin\theta_i\}}{\partial Q_l}(V_i\cos\theta_i + \mathrm{j}\,V_i\sin\theta_i)\Big) \\
&= \frac{1}{V_i}\left(V_i\cos\theta_i\frac{\partial(V_i\cos\theta_i)}{\partial Q_l} + V_i\sin\theta_i\frac{\partial(V_i\sin\theta_i)}{\partial Q_l}\right) \\
&= \frac{1}{V_i}\mathrm{Re}\left(\underline{V}_i\frac{\partial\overline{V}_i}{\partial Q_l}\right).
\end{aligned} \tag{42}$$

According to (40), we can obtain,

$$\begin{aligned}
\mathrm{Im}\left(\underline{V}_i\frac{\partial\overline{V}_i}{\partial Q_l}\right) &= V_i\cos\theta_i\frac{\partial\{V_i\sin\theta_i\}}{\partial Q_l} - V_i\sin\theta_i\frac{\partial\{V_i\cos\theta_i\}}{\partial Q_l} \\
&= V_i\left(V_i\cos^2(\theta_i)\frac{\partial\theta_i}{\partial Q_l} + V_i\sin^2(\theta_i)\frac{\partial\theta_i}{\partial Q_l}\right) \\
&= V_i^2\frac{\partial\theta_i}{\partial Q_l}.
\end{aligned} \tag{43}$$

Thus, we can obtain,

$$\frac{\partial\theta_i}{\partial Q_l} = \frac{1}{V_i^2}\mathrm{Im}\left(\underline{V}_i\frac{\partial\overline{V}_i}{\partial Q_l}\right). \tag{44}$$

9. References

[1] Wind energy scenarios for 2030, European Wind Energy Association. [Online]. Available: https://windeurope.org/fileadmin/files/library/publications/reports/EWEA-Wind-energy-scenarios-2030.pdf

[2] Xu, L., Yao, L.: 'DC voltage control and power dispatch of a multi-terminal HVDC system for integrating large offshore wind farms', *IET Renew. Power Gener.*, 2011, 5, (3), pp. 223–233

[3] Guo, Y., Gao, H., Wu, Q.: 'A combined reliability model of VSC-HVDC connected offshore wind farms considering wind speed correlation', *IEEE Trans. on Sustain. Energy,* in press

[4] Xu, L., Yao, L., Sasse. C.: 'Grid integration of large DFIG-based wind farms using VSC transmission', *IEEE Trans. Power Syst.*, 2007, 22, (3), pp. 976-984
[5] Z. Zhang, Y. Sun, D. Gao, *et al.*: 'A versatile probability distribution model for wind power forecast errors and its application in economic dispatch', *IEEE Trans. Power Syst.*, 2013, 28, (3), pp. 3114-3125
[6] Wang, S., Han, L. Wu, L.: 'Uncertainty Tracing of Distributed Generations via Complex Affine Arithmetic Based Unbalanced Three-Phase Power Flow', *IEEE Trans. Power Syst.*, 2015, 30, (6), pp. 3053-3062
[7] Mohseni M., Islam, S. M.: 'Review of international grid codes for wind power integration: Diversity, technology and a case for global standard', *Renewable Sustain. Energy Rev*., 2012, 16, pp. 3876-3890
[8] Firouzi, M., Gharehpetian, G. B., Mozafari, B.: 'Power Flow Control and Short Circuit Current Limitation of Wind Farms Using Unified Inter-Phase Power Controller', *IEEE Trans. Power Del*., 2017, 32, (1), pp. 62-71
[9] Karthikeya, B. R., Schutt, R. J.: "Overview of wind park control strategies," *IEEE Trans. on Sustain. Energy*, 2014, 5, (2), pp. 416-422
[10] Guo, Q., Sun, H., Wang, B., Zhang, B., Wu, W., Tang, L.: 'Hierarchical automatic voltage control for integration of large-scale wind power: Design and implementation', *Electr. Power Syst. Res.*, 2015, 120, pp. 234-241
[11] Zhao, H., Wu, Q., Guo, Q., Sun, H., Huang, S., Xue, Y.: 'Coordinated voltage control of a wind farm based on model predictive control', *IEEE Trans. Sustain. Energy*, 2016, 7, (4), pp. 1440–1451
[12] Demirovic, N.: 'Impact of statcom and SVC to voltage control in systems with wind farms using induction generators (IG)', *Mediterranean Conference on Power Generation, Transmission, Distribution and Energy Conversion (MedPower)*, Belgarde, Serbia, Nov., 2016 pp. 1-6
[13] Pulgar-Painemal, H. A., Gálvez-Cubillos, R. I.: 'Limit-induced bifurcation by wind farm voltage supervisory control', *Electr. Power Syst. Res.*, 2013, 103, pp. 122-128
[14] Moawwad, A., El Moursi, M. S., Xiao, W., Kirtley, J. L.: 'Novel configuration and transient management control strategy for VSC-HVDC', *IEEE Trans. Power Systs*., 2014, 29, (5), pp. 2478-2488
[15] Kirakosyan, A., Elmoursi, M., Khadkikar, V.: 'Fault Ride Through and Grid Support Topology for the VSC-HVDC Connected Offshore Wind Farms', *IEEE Trans. Power Del*., 2017, 32, (3), pp. 1592-1604
[16] Van Der Meer, A. A., Ndreko, M., Gibescu, M., van der Meijden, M. A.: 'The effect of FRT behavior of VSC-HVDC-connected offshore wind power plants on AC/DC system dynamics', *IEEE Trans. Power Del*., 2016, 31, (2), pp. 878-887
[17] Muyeen, S. M., Takahashi, R., Tamura, J.: 'Operation and control of HVDC-connected offshore wind farm', *IEEE Trans. Sustain. Energy*, 2010, 1, (1), pp. 30-37
[18] Martnez, J., Kjar, P. C., Rodriguez, P.: 'Comparison of two voltage control strategies for a wind power plant', *Proc. IEEE/PES Power Syst. Conf. Expo. (PSCE)*, 2011, pp. 1-9.
[19] Cole, S., Beerten, J., Belmans, R.: 'Generalized dynamic VSC MTDC model for power system stability studies', *IEEE Trans. Power Syst.*, 2010, 25, (3), pp. 1655-1662
[20] Christakou, K., LeBoudec, J. Y., Paolone, M., Tomozei, D. C.: 'Efficient computation of sensitivity coefficients of node voltages and line currents in unbalanced radial electrical distribution networks', *IEEE Trans. Smart Grid*, 2013, 4, (2), pp. 741–750
[21] Lagonotte, P., Leost, J. C., Paul, J. P.: 'Structural analysis of the electrical system: Application to secondary voltage control in France', *IEEE Trans. Power Syst.*, 1989, 4, (2), pp. 479-486.
[22] Grunnet, J. D., Soltani, M., Knudsen, T., Kragelund, M. N., Bak, T. "Aeolus toolbox for dynamic wind farm model, simulation and control," in Proc. Eur. Wind Energy Conf., 2010, pp. 1–6.